

Validation of a handheld polarized hyperspectral imaging probe on intralipid phantom and mouse tissue

Jeremy C. Sherey^{a,†}, Ling Ma^{a,b,†}, Amie M. Ha^{a,b}, Cooper Lane^{a,b}, Baowei Fei^{a,b,c,*}

^a Center for Imaging and Surgical Intervention, University of Texas at Dallas, Richardson, TX

^b Department of Bioengineering, University of Texas at Dallas, Richardson, TX

^c Department of Radiology, University of Texas Southwestern Medical Center, Dallas, TX 75390

[†]Equal contribution, *Corresponding author: bfei@utdallas.edu, Website: <https://fei-lab.org>

ABSTRACT

In this study, we designed a handheld polarized hyperspectral imaging (PHSI) system capable of full Stokes imaging. To enable *in vivo* utilization, we validated the PHSI system in Intralipid phantoms, *ex vivo* burned tissues, and various *ex vivo* organ tissues from mice. A calibration experiment was carried out using a quarter-wave plate and a half-wave plate as samples. The errors introduced by the optical components and the camera were analyzed, respectively. Using a phantom composed of varying concentrations of Intralipid solution and methylene blue as a scattering and absorbing agent, the ability of the probe to detect different levels of light scattering was assessed. Eighteen samples were used with Intralipid concentrations varying from 1 to 12 ml and methylene blue with concentrations from 0 to 4 ml. These trials resulted in a correlated trend between the concentration of the Intralipid solution and the intensity of polarization metrics. Additional validation of the system was conducted on burned *ex vivo* mouse muscle tissues. The results of burn tissue experiments showed visible differences in burned and non-burned tissue. Finally, images of mouse organs acquired using the probe showed different levels of light scattering, proving that our probe could reveal the structural differences among tissue types.

Keywords: Polarized hyperspectral imaging (PHSI), handheld, polarization, calibration, Intralipid phantom, burned tissue

1. INTRODUCTION

Polarized hyperspectral imaging (PHSI) is an optical imaging technique that captures images across a broad spectrum of wavelengths and utilizes polarized light to detect variations in tissue structure and composition.^{1, 2} This method is a combination of hyperspectral imaging (HSI) and polarized light imaging (PLI) that provides data on tissue properties such as scattering and molecular composition, which are largely undetectable by conventional imaging.¹ PHSI has been used for medical diagnostics and tissue structure analysis,^{3, 4} but despite its potential its usage has been restricted by the size and complexity of current systems. However, a handheld system could remove this limitation and expand its applications to clinical environments where a compact device and real-time imaging would provide a powerful tool for diagnosis.

Burn injuries are a common result of thermal exposure, exhibiting significant changes in optical properties due to alterations in tissue structure and composition. Burns typically affect the scattering and absorption characteristics of tissues, which can be detected and analyzed using advanced imaging techniques like PHSI. Studying burned tissue is crucial for improving the diagnosis, monitoring, and treatment of burn injuries, as well as for understanding the underlying mechanisms of tissue damage and repair. By detecting and characterizing these changes, PHSI can provide valuable insights into burn severity, tissue healing, and treatment outcomes. Using mouse skin and organs burned in variations of exposure time, we can begin to gain insights into whether a handheld system shows promise in detecting these changes. By exploring the capabilities of PHSI in these contexts, this study seeks to advance the development of portable, non-invasive imaging systems that can enhance diagnostic accuracy and improve clinical outcomes in tissue analysis.

In our previous study, an automated PHSI setup with full Stokes imaging capability was implemented for fast, non-contact, and non-invasive tissue assessment.¹ It had two fixed branches with no manual rotating component and can acquire images within two seconds. We conducted preliminary testing on *ex vivo* mouse tissue samples and calculated polarization metrics such as degree of polarization (DOP), degree of linear polarization (DOLP), and degree of circular polarization (DOCP), which validated the feasibility of tissue assessment using PHSI. In the current work, we evaluated the spectral performances of the system and assembled the system into one light-weight handheld PHSI probe, which was validated using intralipid solution of various concentrations as well as various *ex vivo* mouse tissues.

2. METHODS

2.1 Handheld PHSI Probe

In our previous study, we developed a PSHI system with an illumination branch and an imaging branch. Despite the relatively compact design of the entire system, its portability needed to be improved. Its capability of imaging at different angles was lacking. In order to improve the versatility of the system, we modified it into a light-weight handheld PHSI probe. Specifically, we replaced the light-emitting diode (LED) source and linear polarizer (LP) in the illumination branch with a compact ring light and a ring-shaped linear polarizer, which were attached to the distal end of the imaging probe, as shown in Figure 1. The imaging probe consists of two liquid crystal variable retarders (LCVR), a linear polarizer, and a focus lens. A snapshot camera is attached at the proximal end of the probe. By layering these components together and varying the driving voltages of the LCVRs, the system can achieve full Stokes imaging. The transmissive axis of the first polarizer (in front of light source) was placed at 45° orientation, and the second polarizer was set at 0° . The fast axis of the first LCVR was orientated at 0° , while the second LCVR was orientated at 45° . All optics were housed in a 3D printed probe shell, which had threads on both ends for the ring light and snapshot camera to be tightly attached. The working distance of the PHSI probe was carefully calculated by combining the focal length of the lens and the working distance of the ring light. An additional tube was 3D-printed and placed around the ring light to block the ambient light. All 3D printed parts used matt black PLA filaments, which minimized reflection or ambient light. Software to control the system has been developed based on the application programming interfaces (API) of the LCVRs and the camera.¹ In our software, we implemented various image acquisition modes, including automatic acquisition of all four intensity images and the reference image as well as the manual acquisition of a single intensity image. After the acquisition, the software can also perform data processing for reference calibration, calculation of Stokes parameters, as well as the polarization metrics DOP, DOLP, and DOCP. The automatic acquisition takes about one second and image processing within ten seconds.

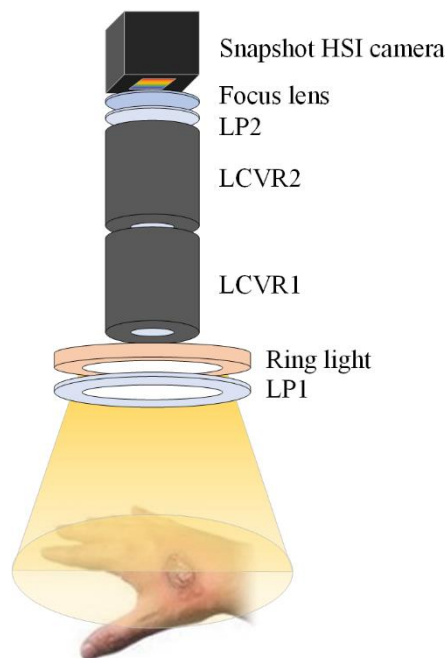


Figure 1. Diagram of the PHSI probe. LP: linear polarizer; LCVR: liquid crystal variable retarder.

2.2 PHSI Probe Calibration Experiments

Despite our work in manually aligning the components, error within the system was inevitably introduced by the angular positions of the axes of multiple optical components, different values of the retardance of each LCVR caused by suboptimal driving voltages, and other effects such as the optical response of the LCVRs. In order to evaluate the experimental errors of the PHSI probe, we carried out a series of experiments. The setup includes a broadband xenon light source with fiber guide, a linear polarizer placed after the light fiber guide with its transmissive axis at 45° orientation, a sample, the PHSI probe, and a light detector. The 45° oriented linear polarizer polarizes the incident light beam, which then shines on the sample and goes through the polarization analyzer (LCVR1, LCVR2, and LP2) before reaching the light detector.

The experiment was conducted in two stages. The first stage of the experiment was performed using only the polarization analyzer without the hyperspectral camera. A high-sensitivity and high-resolution spectrometer served as the light detector and was placed after the probe to measure the intensities of the light at multiple wavelengths, as shown in Figure 2. This stage assesses the errors from the polarization components, which are the major source of errors in this setup. For the second stage, the spectrometer was replaced with the actual snapshot hyperspectral camera that measured light intensities over 16 spectral bands in the wavelength range of 460-600 nm. By comparing the Stokes vectors measured by the spectrometer and the hyperspectral camera, we could evaluate the experimental error introduced by the hyperspectral camera.

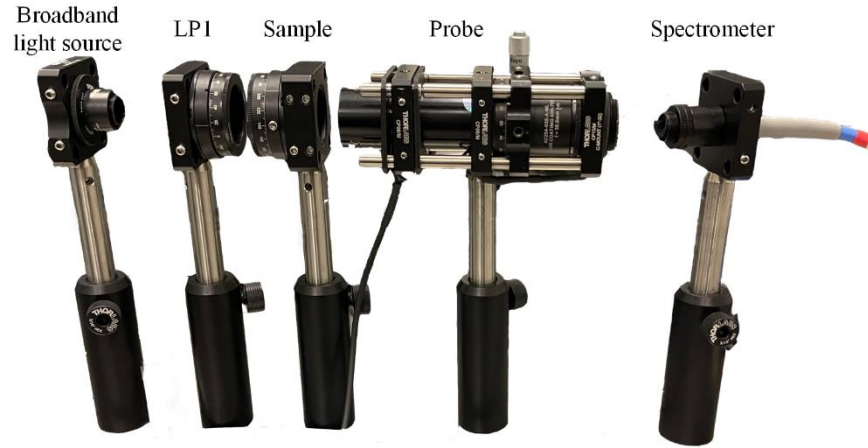


Figure 2. Experimental setup for polarized hyperspectral imaging with spectrometer.

For each stage of the experiment, two samples, *i.e.*, a half-wave plate and a quarter-wave plate, were employed separately. The fast axis of the waveplate was rotated from 0° to 180° with a 10° increment.⁵ At each step, different driving voltages were applied to the LCVRs and a set of four intensity values, *i.e.*, I_H , I_V , I_{45} , and I_{LC} , were acquired, which were then used to calculate the Stokes parameters.¹ When using the spectrometer, a set of four spectra were saved; while for the hyperspectral camera, four images were saved and later the intensity values of each spectral band are extracted from the images. Theoretical values of Stokes parameters for each axis angle were also calculated based on the Mueller matrix of each component as a reference to compare with the experimental values, as shown by Equations (1-2):

$$S_{\lambda/2} = \begin{pmatrix} 1 \\ \sin 4\theta \\ -\cos 4\theta \\ 0 \end{pmatrix} \quad (1)$$

$$S_{\lambda/4} = \begin{pmatrix} 1 \\ \sin 2\theta \cos 2\theta \\ \sin 2\theta \sin 2\theta \\ -\cos 4\theta \end{pmatrix} \quad (2)$$

where θ is the rotating angle at each step, $S_{\lambda/2}$ is the theoretical Stokes vector of the half-wave plate at θ , and $S_{\lambda/4}$ is the theoretical Stokes vector of the quarter-wave plate at θ .

Once the experimental values of Stokes parameters were obtained, the root mean square error (RMSE) was used as a measure of the experimental error of the PHSI system, as in Equation (3):

$$RMSE = \sqrt{\frac{1}{N_\theta} \sum_{n=1}^{N_\theta} (S_{i,n}^{exp} - S_{i,n}^{theory})^2} \quad (3)$$

where $N_\theta = 19$ is the total number of rotating angles θ from 0° to 180° with 10° increments; $S_{i,n}^{exp}$ ($i = 0, 1, 2, 3$) and $S_{i,n}^{theory}$ ($i = 0, 1, 2, 3$) are the experimental and theoretical values of Stokes parameters at the n -th angle.

2.3 Intralipid Phantom Validation

After using the abovementioned experiment to confirm that the system follows general intensity and Stokes parameter trends, we assembled the illuminator, LCVR1, LCVR2, LP2, and snapshot hyperspectral camera into the handheld probe. To further validate the assembled probe, we carried out experiments using Intralipid (IL) phantoms. Intralipid is a fat-based solution composed primarily of soybean oil, phospholipids, and glycerin, which is comparable with biological tissue scattering properties. Combining IL with absorbing agents like methylene blue (MB) allows for a highly controlled environment that replicates a wide range of tissue characteristics. This makes intralipid phantoms a valuable tool for validating imaging systems like PHSI. By varying the concentration of IL and MB, we can closely simulate different tissue types.

For this experiment we used an intralipid 20% fat emulsion to create the phantom experimental groups. We began by preparing a MB stock solution at $400 \mu\text{M}$. First calculating the amount in grams of MB powder needed to mix with distilled water to achieve the desired concentration for our absorbing agent. After determining the number of moles required for the solution, we found that 0.05 grams of MB powder were used with 0.39 L distilled water. Alternatively, the absorption solution can be made using controlled dilutions of the MB stock solution in small volumes to achieve the desired concentration using a small amount of MB powder and distilled water.

As a preliminary test we made multiple IL phantom samples. After the phantoms were constructed, imaging was conducted to determine whether the PHSI system could distinguish between the variations in concentration of IL emulsion and MB solution. To the human eye, there might not be much observable difference between the various concentrations of IL that contained 0 ml of MB, as they all appeared a consistent milky white. We labeled 18 cells of well plates according to the volumes and combinations of IL and MB solutions. The containers were laid in a four-by-four grid with the columns increasing in the volume of IL starting on the left from 1 ml to 2 ml to 4 ml to 8 ml, and rows increasing in MB solution volume starting at the top going from 0 ml to 1 ml to 2 ml to 4 ml. The last two samples in this experiment (top right and bottom left) contained 12 ml of only IL in one and MB in the other, which was to get a baseline for their scattering and absorption properties, respectively. Each sample's total volume was brought to 12 ml when necessary, which was achieved by supplementing any low volume samples with distilled water that had negligible impact on the scattering properties of the phantoms. Once all the ingredients were added to each container, we mixed the solutions using a stirring rod.

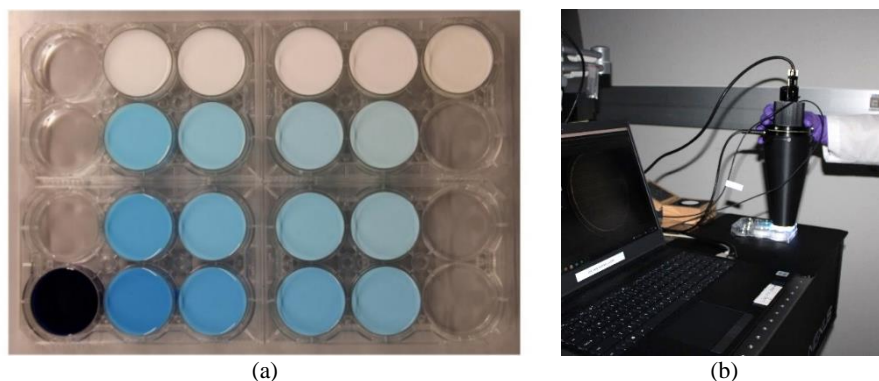


Figure 3. Validation of the PHSI probe with intralipid phantom samples. (a) Phantoms with various volumes of Intralipid emulsion and methylene blue. The top right sample contains 12 mL of 20% IL emulsion with no MB. The bottom left sample contains only MB solution. (b) Imaging the samples using the handheld probe.

2.4 Ex Vivo Tissue Experiment

Additionally, we used various *ex vivo* tissue samples to ensure that the PHSI setup can differentiate between tissue structures. System validation on biological tissues was conducted using different types of mouse tissues and organs, as well as burned muscle tissues. All tissues were collected from euthanized mice. We intended to implement a qualitative comparison of Stokes vectors from different tissue types to validate the function of the PHSI probe. Biological samples exhibit realistic optical properties, which are essential for validating how the system will perform in practical scenarios. Since the polarization signal can be affected by the sample's surface roughness, thickness, and internal structure, using actual tissue samples can help test the system's response to these variables and refine its calibration and accuracy.

For each euthanized mouse, we harvested the heart, muscle, lung, intestine, and liver and immediately imaged the samples individually with the probe. Then, the muscles were burned with a soldering iron for a certain amount of time. The handheld PHSI system, due to its mobility, allowed for easier access to imaging fresh tissue samples. The probe was simply placed over the sample and captured all images of the tissues which were being housed in small containers.

Table 1. Different properties of tissues that affect light depolarization.

| | Heterogeneity | Scattering | Anisotropy | Birefringence |
|-----------|---------------|-----------------|----------------|---------------|
| Heart | Moderate | Moderate | Moderate | Moderate |
| Liver | Moderate | High | Low - Moderate | Negligible |
| Lung | High | Moderate - High | Low | Negligible |
| Intestine | Very high | High | Low | Low |
| Muscle | Low | Moderate | High | High |

3. RESULTS

3.1 PHSI Probe Error Measurement

To verify the developed system and measure the systematic errors, we carried out experiments using two samples, *i.e.*, a half-wave plate and a quarter-wave plate, by rotating the fast axes of the samples from 0° to 180° with 10° increments. The four intensity images, namely I_H , I_V , I_{45} , and I_{LC} , were recorded and then used to calculate the experimental values of Stokes parameters at each angle.

Figure 4 shows how the Stokes parameters S_1 , S_2 , and S_3 change along with the orientation of the fast axis of the half-wave plate. We first calculated the Stokes parameters using the average of all 16 bands, as shown in the left column in the figure. It can be seen that S_1 and S_2 generally matched the theoretical curves well, especially using the "probe + camera" setup with an RMSE of 0.11 for S_1 and 0.04 for S_2 . The RMSEs of the spectrometer setup were slightly larger, which was likely caused by manual errors during the rotation of the half-wave plate. Since the incident light was linearly polarized, and a half-wave plate only rotates the polarization direction of the linearly polarized light, the S_1 and S_2 Stokes parameters, which described the state of linearly polarized light, were fairly accurate. However, larger errors were observed for the measured Stokes parameter S_3 , which should be theoretically zero at all angles. It could be possibly caused by the misalignment of optical axes or the insufficient attenuation of the incoming linear polarized light. Nevertheless, this error can be corrected by using a nonlinear fitting procedure, which minimizes the sum of differences between the experimental intensities and the theoretical values.⁵ Furthermore, we extracted two spectral bands, *i.e.*, 500 nm and 575 nm, from all 16 bands in the 460-600 nm wavelength range, to analyze the spectral errors of the Stokes parameters, as shown in middle and right columns in Figure 4. It is obvious that for both Stokes parameters, the system had less errors at the longer wavelength (575 nm) than the shorter wavelength (500 nm), regardless of whether it was using the spectrometer or the camera. Note that the LCVR components were calibrated using a laser of a longer wavelength. Therefore, the dispersion of retardance across the wide spectral range led to wavelength-dependent errors. In the future, we will carry out calibration at various wavelengths to correct the wavelength dependency.

Figure 5 shows the experimental and theoretical Stokes parameters for a rotating quarter-wave plate. A quarter-wave plate converts the incident linear polarized light to elliptically or circularly polarized light when there is an angle between the light polarization and the optical axis of the wave plate. It can be seen that the experimental curves of S3 using both setups aligned well with the theoretical curve, with a RMSE of 0.12 using the spectrometer and 0.14 using the camera, indicating the capability and accuracy of our developed system to detect elliptically and circularly polarized light. However, the experimental curves of S1 and S2 showed more systematic errors including a shift along the X axis and asymmetry. A similar condition was reported in a previous study,⁵ where the errors were corrected using nonlinear fitting and the RMSEs lowered to an acceptable level. In the future, we will carry out software calibration to eliminate the errors. Table 2 lists all the RMSEs values using both setups for two samples.

Table 2. RMSE of experimental Stokes parameters of two samples.

| | | S1 | S2 | S3 |
|--------------------|--------------|------|------|------|
| Half-wave plate | Spectrometer | 0.14 | 0.22 | 0.58 |
| | Camera | 0.11 | 0.04 | 0.68 |
| Quarter-wave plate | Spectrometer | 0.15 | 0.21 | 0.12 |
| | Camera | 0.17 | 0.12 | 0.14 |

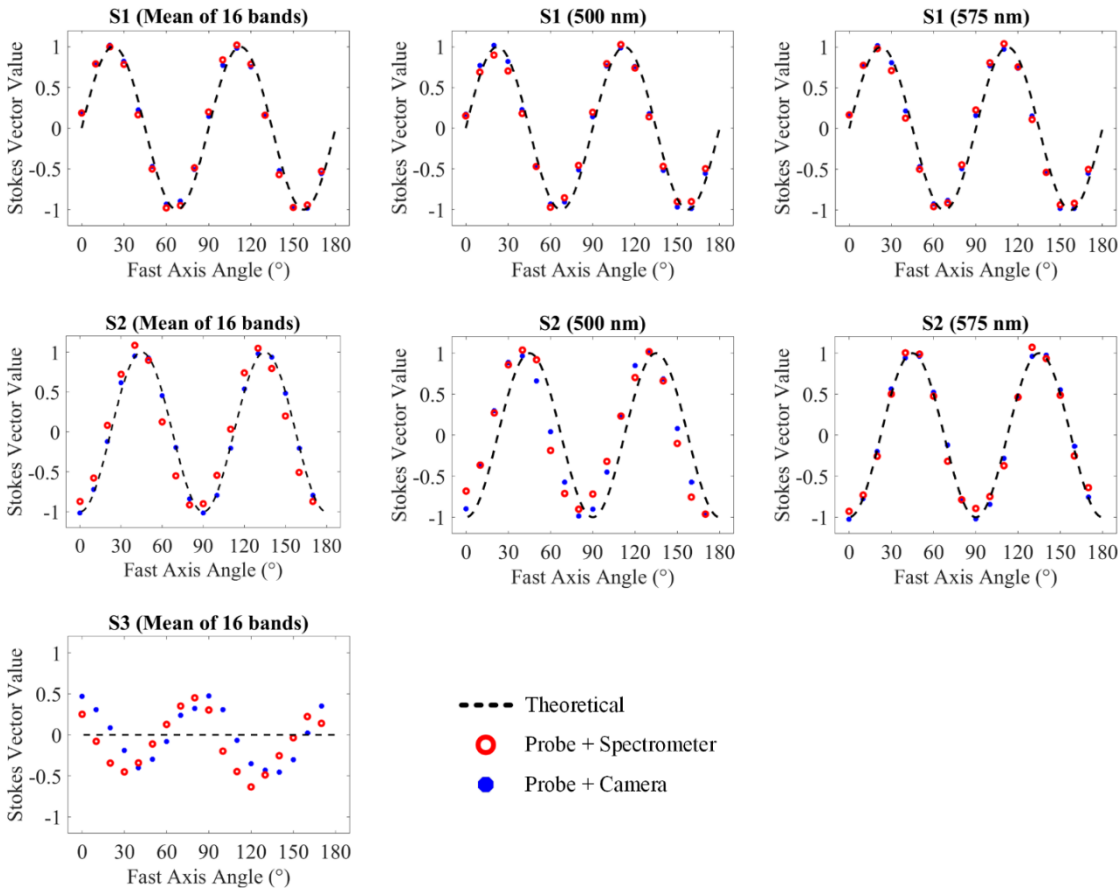


Figure 4. Stokes parameters from the spectrometer and camera for the *half wave plate* sample. The theoretical values are shown as dash lines, and the experimental values using the two setups (one with the spectrometer and the other with the snapshot hyperspectral camera) were shown with red circles and blue dots, respectively.

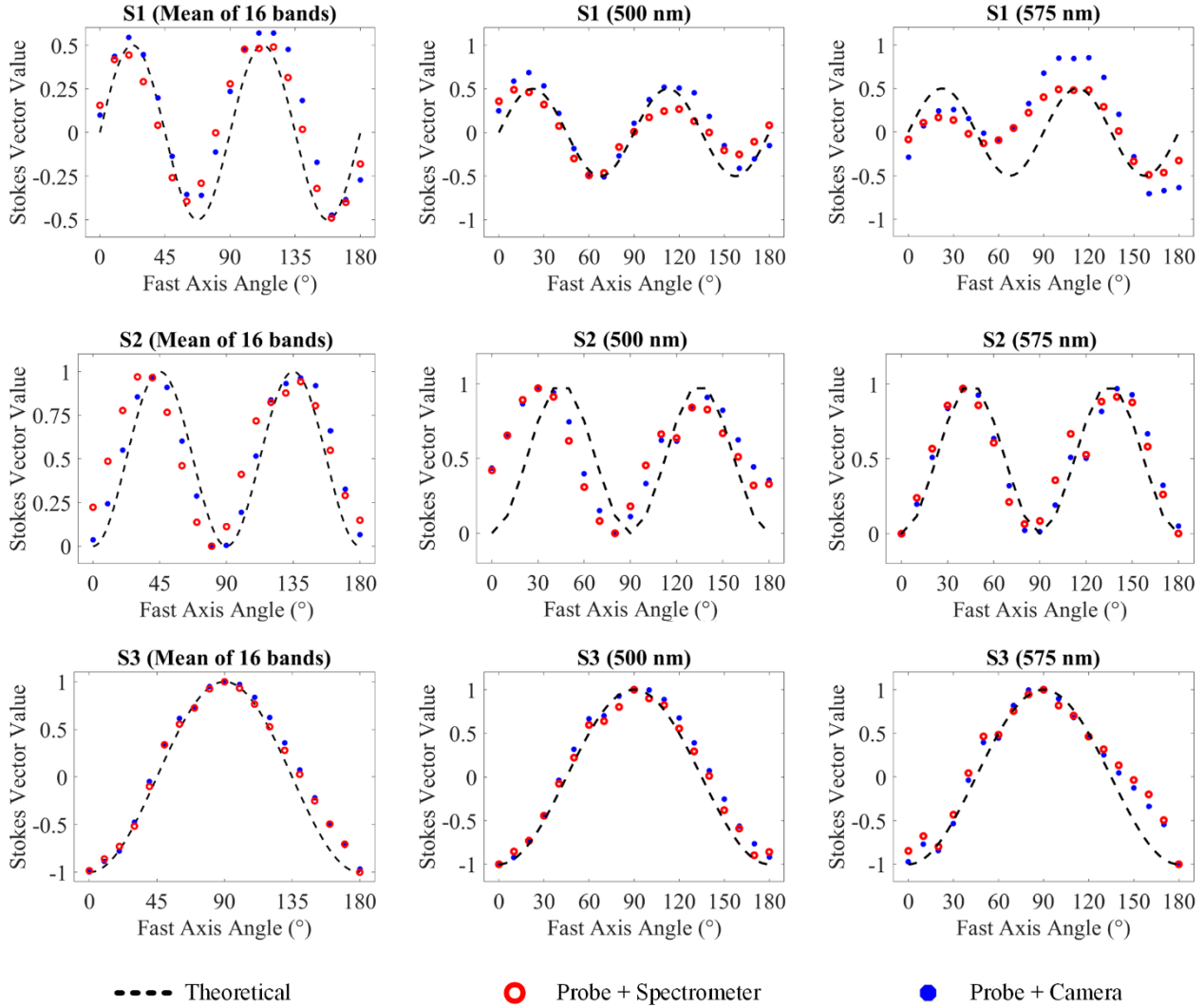


Figure 5. Stokes parameters from the spectrometer and camera for the *quarter-wave plate* sample. The theoretical values are shown as dash lines, and the experimental values using the two setups (one with the spectrometer and the other with the snapshot hyperspectral camera) were shown with red circles and blue dots, respectively.

3.2 Intralipid Phantom Validation

To validate the feasibility of polarization-sensitive detection using our probe, we prepared phantoms using 20% Intralipid emulsion solution as a scattering agent and the methylene blue as an absorbing agent. A total of 18 phantom samples were made, with one phantom only containing the 20% Intralipid emulsion, one phantom only containing the methylene blue solution, and the rest containing a combination of both with various concentrations. As a reference, all intensity images, *i.e.*, I_H , I_V , I_{45} , and I_{LC} , of the sample with merely methylene blue solution had very low intensities, since methylene blue mainly serves as an absorbing agent. The DOP, DOLP, and DOCP values of that sample were also close to zero, indicating minimal scattering effects from the methylene blue.

Our PHSI probe revealed clear differences when increasing concentration of IL and MB, shown in Figure 6. The 3D visualization allows us to see both concentrations of IL and MB, as well as the relationship between them and the measured values simultaneously. Their relationship is not linear but follows a general trend of increasing in intensity and decreasing in polarization as IL concentration increases and MB decreases. This trend was consistent across all the intensity images

and polarization metrics, indicating the ability of our probe to quantify the differences of scattering properties among samples.

In Figure 6, we could observe a positive correlation between the intensities of I_H , I_V , I_{45} , and I_{LC} and the concentration of IL, regardless of the amount of MB. Since Intralipid emulsion is a milky white liquid, and the lipid droplets have high scattering, a higher concentration of fat particles would increase the intensity of both the reflected and scattered light. Meanwhile, due to the random orientation of fat droplets, a higher concentration of IL significantly depolarizes the linearly polarized incident light, resulting in a lower DOP of the detected backscattered light. Thus, a negative correlation between IL concentration and polarization metrics, *i.e.* DOP, DOLP, and DOCP, were observed in Figure 6, especially when Intralipid volume increased from 1 ml to 4 ml. Since our sample was ~ 10 mm thick, multiple scattering might have had some impacts as well. In the future, we will make thin phantoms to reduce multiple scattering and validate the scattering detection using our probe.

On the other hand, when methylene blue was added to the phantoms, it absorbed some of the incident light, reduced the light reflection and multiple scattering, thus the intensity of I_H , I_V , I_{45} , and I_{LC} got lower, but the polarization state of the backscattered light was better maintained. Figure 7 further proves the impact of methylene blue as an absorbing agent. Methylene blue has stronger absorption in the wavelength range of 550~600 nm compared to 400~500 nm.⁶ Therefore, a significant decrease of detected light intensity, *e.g.*, I_{45} , is observed with the increasing concentration of methylene blue, especially in the longer wavelength range, whereas the calculated polarization metrics show the opposite trend.

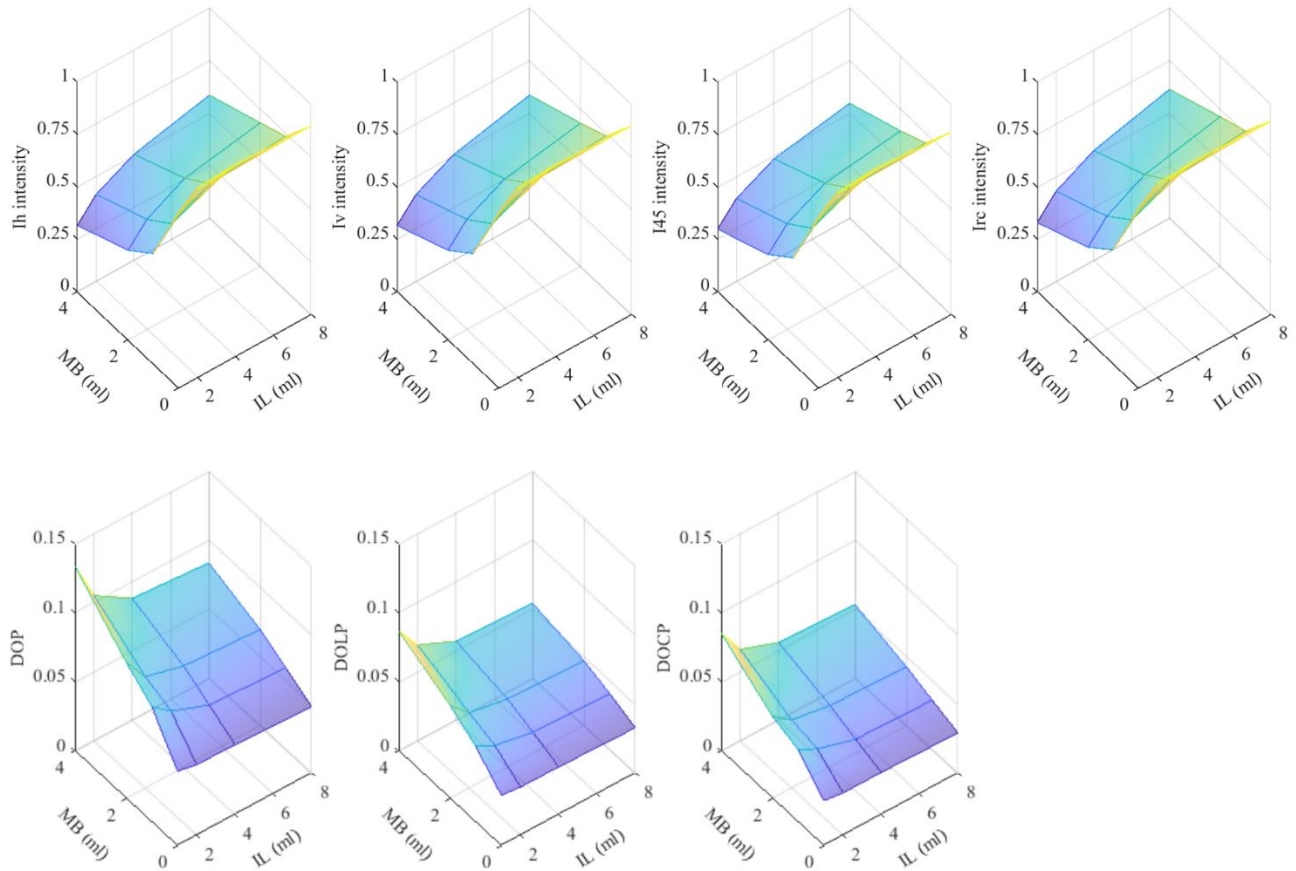


Figure 6. Stokes elements and polarization measurements at different concentrations of intralipid and methylene blue.

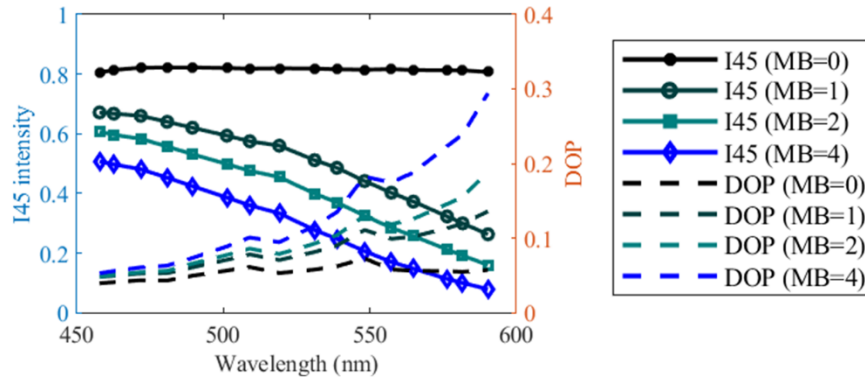


Figure 7. Spectral signatures change of I_{45} and DOP along with methylene blue. MB=0, 1, 2, and 4 are the volumes (ml) of pre-made methylene blue solution.

3.3 *Ex vivo* tissue testing

We tested our assembled handheld PHSI probe on *ex vivo* mouse tissues to validate the capability of tissue characterization of our developed system. Five mice were collected from the Laboratory Animal Resources Center (LARC) of our institution after they were euthanized. Then, the mice were immediately dissected to harvest several organs, which were kept in phosphate-buffered saline (PBS) and transferred to the lab for imaging. After scanning the fresh tissues with our probe, we burned the muscle tissues with a heated soldering iron and imaged the tissues again for comparison. For all samples, we acquired all intensity images and calculated Stokes parameters as well as polarization metrics including DOP, DOLP, and DOCP. The metrics were averaged across all mice and compared, as shown in Figure 8. Note that the mice might have gone through different procedures that induced certain conditions before they were used for the imaging experiments. Therefore, the comparison is to validate the feasibility of tissue assessment, while the polarization metrics shown here may vary among different mice.

Testing on *ex vivo* mouse tissues revealed distinct scattering and depolarization characteristics for different organs. The heart exhibited organized and aligned fibers with minimal depolarization, thus a significantly high DOLP was observed. In addition, fibrotic myocardial tissues tend to have higher DOLP than healthy ones.⁷ Intestine, on the contrary, had high heterogeneity that caused significant scattering and depolarization of the light. The relatively homogeneous optical properties and less organized structure of liver helped preserve the polarization, while the complex air-tissue interfaces in lungs caused comparatively more scattering and depolarization. Interestingly, muscle, which has a highly ordered structure such as the alignment of muscle fibers, showed strong depolarization in our experiments. Considering the thickness of our tissue samples, possible reasons include multiple scattering due to the translucency of muscles or the misalignment between incident light and intrinsic tissue birefringence.⁸ Moreover, the lower DOP of muscle and higher DOP of liver align with the results from our previous study.¹ In the future, we will investigate more about the characterization of the listed organs for a comprehensive comparison, however, the significant high DOLP of heart tissues and the different DOPs among organs in this study reveal the potential of this system for tissue assessment and disease detection.

Finally, for burned tissue, we investigated four Stokes parameters as well as three polarization metrics. It was found that the burned area, as shown by the red arrow in Figure 9, had changes in the polarization. Thanks to the destruction of fiber structures and the increased heterogeneity in burned muscle tissues, the comparison of heatmaps of Stokes parameter S_2 and DOLP reveals obviously different values between healthy and burned tissues while other unaffected regions, highlighting the probe's diagnostic potential. The current heatmap provides high contrast between healthy and burned tissues in a qualitative way, but we may investigate the feasibility of burn degree measurement using PHSI in the future.

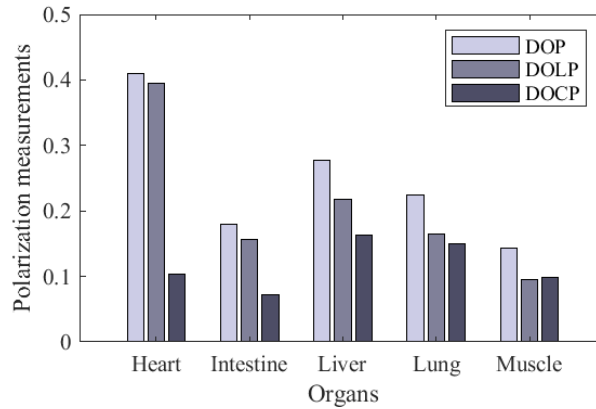


Figure 8. Polarization measurements of different organs.

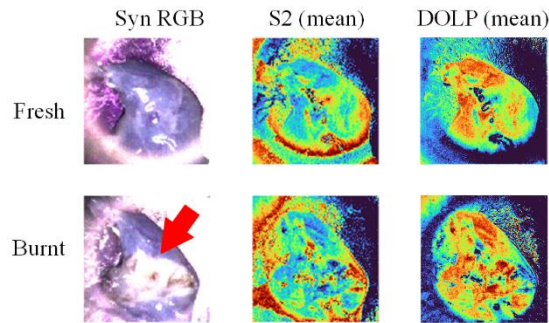


Figure 9. Stokes vector S_2 and DOLP detect burn in mouse tissue. The red arrow indicates the burned tissue area, where Stokes parameter S_2 and polarization metric DOLP showed heterogeneous values that are different from those of healthy tissues.

4. DISCUSSION & CONCLUSION

In this study, we developed a lightweight handheld probe for *in vivo* polarized hyperspectral imaging. Various calibration experiments were carried out, where the systematic errors of the probe were measured, and the wavelength-dependency was analyzed. To validate the constructed probe, we first employed Intralipid phantoms with varying concentrations of Intralipid as the scattering agent and methylene blue as the absorbing agent. A negative correlation between the DOP of the detected backscattered light and the concentration of Intralipid was observed due to the strong scattering and depolarization of fat droplets, whereas the increasing concentration of methylene blue would reduce the reflection and multiple scattering, resulting in preservation of polarization states of the light. Next, we tested the probe on fresh *ex vivo* mouse organs and burned muscle tissues to validate this system in biological tissues. The results showed that our probe could reveal different characteristics of biological samples and tissue burns. In evaluating the efficacy of the handheld probe, many desired features were successfully implemented. Although there is room for improvement with the margins of error between the real and theoretical Stokes parameters, we have found that our system performs proficiently, especially in the cases of providing contrast between structures and differentiating levels of scattering properties of different tissue and various phantoms.

For the future iterations of this work, we will first decrease the systematic error until it is negligible. We will modify the mechanical design of the probe for a precise alignment of the optical axes of components. Meanwhile, software calibration will be carried out to minimize the discrepancies between experimental measurements and theoretical values. In addition, we will improve the Intralipid phantom validation experiment. A thinner phantom will be employed to avoid

multiple scattering, and both the backscattered light and transmitted light will be imaged to assess the polarization measurement capability of our probe. We will test the probe on a larger number of mice with known tissue characteristics. Moreover, polarized hyperspectral imaging with longer wavelengths, *e.g.*, red to near infrared, will be investigated, as tissues tend to preserve polarization better in that range.

Overall, the ease-of-use aspect of the handheld device was useful when compared to our previously developed microscope-based as well as the two-branch PHSI setups. Its compact design allowed for rapid image acquisition of various samples, and the transition time between setting up for the next image was also vastly reduced compared to our polarized hyperspectral microscope² or two-branch PHSI setup¹. Additionally, the systems portability in a clinical environment makes it a simple solution to the need for expedient high-contrast images. The probe's use on burn tissue allowed us to visualize and confirm that the system was detecting changes to tissue structure and light scattering, while also providing a look into how it might handle future applications. We foresee this handheld device being used for detection and diagnosis of cancers and further scientific experimentation into tissue scattering and absorption properties.

ACKNOWLEDGEMENTS

Research reported in this publication was supported in part by the National Cancer Institute of the National Institutes of Health under Award Number R01CA288379 and R01CA204254 and by the Cancer Prevention and Research Institute of Texas (CPRIT) under Award Number RP240289 and RP240542. The content is solely the responsibility of the authors and does not necessarily represent the official views of the National Institutes of Health.

DISCLOSURES

The authors have no relevant financial interests in this article and no potential conflicts of interest to disclose.

REFERENCES

- [1] Ma, L., Srinivas, A., Krishnamurthy, A., Zhou, X., Shah, N. S., Obaid, G., and Fei, B., "Automated polarized hyperspectral imaging (PHSI) for ex-vivo and in-vivo tissue assessment." *Proc. SPIE 12391, Label-free Biomedical Imaging and Sensing (LBIS) 2023*, 123910F (2023).
- [2] Zhou, X., Ma, L., Mubarak, H., Palsgrove, D., Sumer, B., Chen, A., and Fei, B., "Polarized hyperspectral microscopic imaging system for enhancing the visualization of collagen fibers and head and neck squamous cell carcinoma," *Journal of Biomedical Optics*, 29(1), 016005 (2024).
- [3] Vasefi, F., MacKinnon, N., Saager, R. B., Durkin, A. J., Chave, R., Lindsley, E. H., and Farkas, D. L., "Polarization-sensitive hyperspectral imaging in vivo: a multimode dermoscope for skin analysis," *Scientific reports*, 4(1), 1-10 (2014).
- [4] Ghassemi, P., Travis, T. E., Moffatt, L. T., Shupp, J. W., and Ramella-Roman, J. C., "A polarized multispectral imaging system for quantitative assessment of hypertrophic scars," *Biomedical Optics Express*, 5(10), 3337-3354 (2014).
- [5] Montes-González, I., Bruce, N. C., Rodríguez-Herrera, O. G., and Rodríguez Núñez, O., "Method to calibrate a full-Stokes polarimeter based on variable retarders," *Applied Optics*, 58(22), 5952-5957 (2019).
- [6] Fernández-Pérez, A., and Marbán, G., "Visible Light Spectroscopic Analysis of Methylene Blue in Water; What Comes after Dimer?," *ACS Omega*, 5(46), 29801-29815 (2020).
- [7] Bagha, T., Kamal, A. M., Pal, U. M., Mohan Rao, P. S., and Pandya, H. J., "Toward the development of a polarimetric tool to diagnose the fibrotic human ventricular myocardium," *J Biomed Opt*, 27(5), (2022).
- [8] Li, X., Ranasinghesagara, J. C., and Yao, G., "Polarization-sensitive reflectance imaging in skeletal muscle," *Optics Express*, 16(13), 9927-9935 (2008).